Journal of
Synchrotron
Radiation

ISSN 0909-0495

Received 20 July 2006
Accepted 24 January 2007

A monolithic Fresnel bimirror for hard X-rays and its application for coherence measurements

Wolfram Leitenberger[a]* and Ullrich Pietsch[b]

[a]Universität Potsdam, Institut für Physik, Am Neuen Palais 10, D-14468 Potsdam, Germany, and [b]Universität Siegen, FB Physik, 57068 Siegen, Germany. E-mail: leitenberger@uni-potsdam.de

Experiments using a simple X-ray interferometer to measure the degree of spatial coherence of hard X-rays are reported. A monolithic Fresnel bimirror is used at small incidence angles to investigate synchrotron radiation in the energy interval 5–50 keV with monochromatic and white beam. The experimental set-up was equivalent to a Young's double-slit experiment for hard X-rays with slit dimensions in the micrometre range. From the high-contrast interference pattern the degree of coherence was determined.

Keywords: coherent X-rays; double-slit interferometer; refraction index; reflectivity.

1. Introduction

In the last couple of years, numerous methods have been reported for the experimental determination of the degree of coherence of hard X-rays, most of them using two-beam interference (Fezzaa *et al.*, 1997; Lang & Makepeace, 1999; Marchesini *et al.*, 2000; Leitenberger *et al.*, 2001; Paterson *et al.*, 2001), diffraction gratings (Guigay *et al.*, 2004; Pfeiffer *et al.*, 2005) or Fresnel diffraction at a fibre (Kohn *et al.*, 2000). An overview was given by van der Veen & Pfeiffer (2004).

The quantitative characterization of the X-ray beam is of interest for the application of coherent X-rays for imaging, X-ray correlation spectroscopy, characterization of optical elements, wavefronts and others. From the contrast of the experimentally measured interference fringes one can determine the degree of coherence. In the case of Young's experiment, the fringe contrast is a direct measure of the degree of coherence (Born & Wolf, 1999).

A Fresnel bimirror (FBM) for X-rays using two independent mirrors was first proposed and investigated in several articles (Fezzaa *et al.*, 1997; Marchesini *et al.*, 2000). It took advantage of the strong demagnification of the projected length of mirrors which are observed at very small incident angles and act equivalent to narrow slits of micrometre size. A FBM is used preferably at incidence angles below the angle of total external reflection, α_c, of the mirror material and is achromatic at incidence angles below the critical angle. The reflection geometry does not cause problems with unwanted transmission of thin metal foils containing microstructures as was described in a previous article (Leitenberger *et al.*, 2004). In the present paper we discuss a monolithic Fresnel bimirror (Fig. 1) and give a number of new experimental results; the basic principle has already been briefly presented (Pietsch *et al.*, 2005).

Another approach, *i.e.* creating narrow slits of micrometre size, was published recently by Aoki *et al.* (2005). There the reflection of X-rays at thin gold stripes coated on a flat surface was investigated. In the angular interval between the critical angles of the two materials, $\alpha_{c(sub)} < \alpha_i < \alpha_{c(coat)}$, we have a ratio of the two reflection coefficients, $R_{coat}/R_{sub} > 100$. However, outside this angular interval the ratio R_c/R_s is much smaller and causes a weaker contrast of interference fringes.

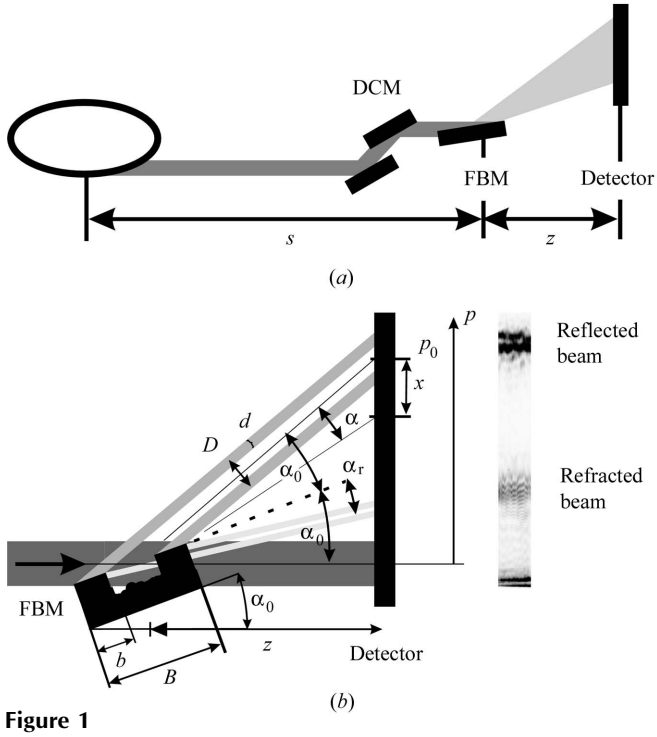

Figure 1
Experimental set-up. (*a*) Beamline set-up. (*b*) Schematic view of the reflected and refracted beams. The angle α is the inclination of the mirror surface to the incident beam. $x = 0$ is the centre of the reflected beam (midpoint beween the two geometrically reflected beams), and angle α_r is in between the refracted beam and the mirror surface. The image on the right-hand side was recorded using 30 keV X-rays at $\alpha = 0.06^\circ$ (the original height of the displayed field of view is 15.4 mm).

In the following we present a FBM where the unnecessary parts of the surface have been completely removed by grinding. The advantage of this layout is in the maximum contrast of the reflected beam between mirror and no mirror. The angular interval of useful operation of the FBM is much wider. In the following considerations we neglect any beam broadening of the slit width caused by penetration of the X-rays into the mirrors.

2. Experimental set-up

The FBM consists of two small mirror planes, each of length b and with separation B, prepared on top of a plane mirror substrate (Fig. 1). The advantage of the set-up presented here compared with the bimirror set-up described by Fezzaa *et al.* (1997) is that both mirrors are already aligned parallel to each other. A single goniometer is sufficient for alignment of the bimirror. The dimensions of the equivalent 'double slit' with an individual slit width d and slit separation D can be modified by changing the angle of incidence α_0. We have $d(\alpha) = b\sin\alpha_0$ and $D(\alpha) = (B - b)\sin\alpha_0$. D is the distance between the midpoints of the two mirrors when assuming two identical mirrors of length b.

For an analytical calculation of the diffraction pattern of the bimirror, one needs to modify the expressions describing the double-slit interferences in order to consider the variable size of the mirrors seen from each position of the detector. Owing to the small incidence angles, we always use in good approximation $\sin\alpha \simeq \alpha$ (with α in radians). In the ideal case the intensity distribution in the far-field diffraction pattern is formed by two completely overlapping stationary optical wavefields diffracted by the two approximated slits, and we obtain (Goodman, 1985)

$$I(x) = I_1(x) + I_2(x) + 2\left[I_1(x)I_2(x)\right]^{1/2}\mu_{12}\cos(k_D x + \varphi), \quad (1)$$

with intensities

$$I_{1,2}(x) = I_{1,2}\,\mathrm{sinc}^2(k_d x \pm D/2).$$

For components $I_{1,2}$ with same amplitudes $I_1 = I_2 = I_0/2$, we obtain

$$I(x) = I_0\,\mathrm{sinc}^2(k_d x)\left[1 + \mu_{12}\cos(k_D x + \varphi)\right] + I_\mathrm{b}. \quad (2)$$

Here,

$$k_d = \frac{\pi b\alpha(x)}{\lambda z} \quad \text{and} \quad k_D = \frac{2\pi B\alpha(x)}{\lambda z} \quad \text{with} \quad \alpha(x) = \alpha_0 + \frac{x}{z}.$$

λ is the wavelength, x is the coordinate in the observation plane normal to the 'slits', where $x = p - p_0$, the distance from a point p in the detector plane to the centre of the diffraction pattern, p_0 is the midpoint of the diffraction pattern for a reflection angle α_0 (the angle between the mirror surface and the centre of the diffraction pattern), φ is the phase angle depending on both the mirror position with respect to the optical axis and the inclination of the mirrors with respect to each other, and I_b is the background intensity. The quantity μ_{12} is the mutual coherence factor describing the degree of coherence between waves reflected by the two mirrors. The visibility V of the interference fringes is defined by

$$V = \frac{I_\mathrm{max} - I_\mathrm{min}}{I_\mathrm{max} + I_\mathrm{min}}. \quad (3)$$

In the case where $I_1 = I_2$, the value of the mutual coherence factor μ_{12} has the same numerical value as the visibility, and for $I_1 \neq I_2$ we have

$$\mu_{12} = \frac{I_1 + I_2}{2(I_1 I_2)^{1/2}} V. \quad (4)$$

The effective slit separation D seen from a position x in the detector plane (at fixed incidence angle α_0) depends on the x position, *i.e.* $D(x) = (B - b)\alpha(x)$. For this reason the fringe spacing in the interference pattern is not constant as in a conventional double-slit experiment; it is larger at the low-angle side of the interference pattern than at the high-angle side (see Figs. 2 and 3).

The aim of the experiment is to determine the fringe visibility as a function of the slit separation and finally to determine the spatial degree of coherence, $\mu_{12}(D)$, between two points, or better slits 1 and 2, in the object plane at distance D from each other over a wide range of energies. Assuming a Gaussian intensity distribution of the source intensity, the degree of coherence probed at the FBM position also has a Gaussian distribution. For a double-slit experiment this quantity can be expressed as a function of the slit separation in the form (Born & Wolf, 1999; Goodman, 1985)

$$\mu_{12}(D) = \gamma\exp\left(-\frac{2\pi D\sigma}{\lambda s}\right)^2 = \gamma\exp\left(-\frac{D^2}{2l_\mathrm{c}^2}\right), \quad (5)$$

where

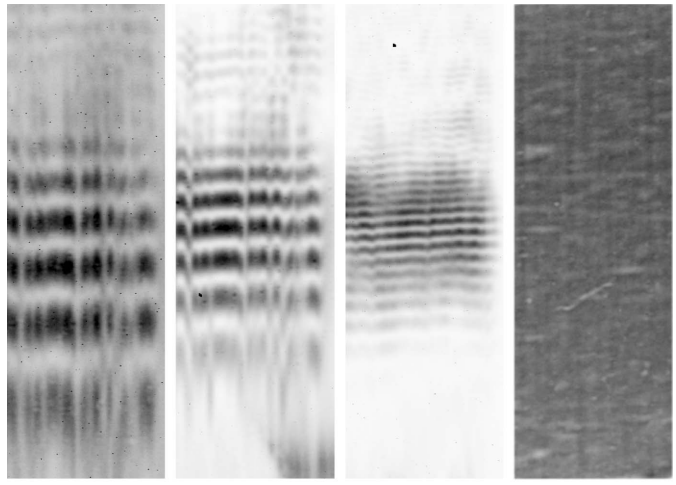

(*a*) (*b*) (*c*) (*d*)

Figure 2
Experimental interference patterns at incidence angle $\alpha_\mathrm{i} = 0.02^\circ$ at different beam energies (*a*) $E = 8$ keV, (*b*) 15 keV and (*c*) 40 keV (wavelength in Å: 1.55, 0.83 and 0.31). (*d*) Transmission image of the direct beam in the region where the FBM is illuminated. The weakly visible vertical stripes cause the additional vertical lines of strong contrast in parts (*a*)–(*c*). Each image shows a field of view of 1.5 mm × 4.5 mm. The vertical offset of the camera was 5 mm in (*a*)–(*c*) and 0 mm in (*d*)

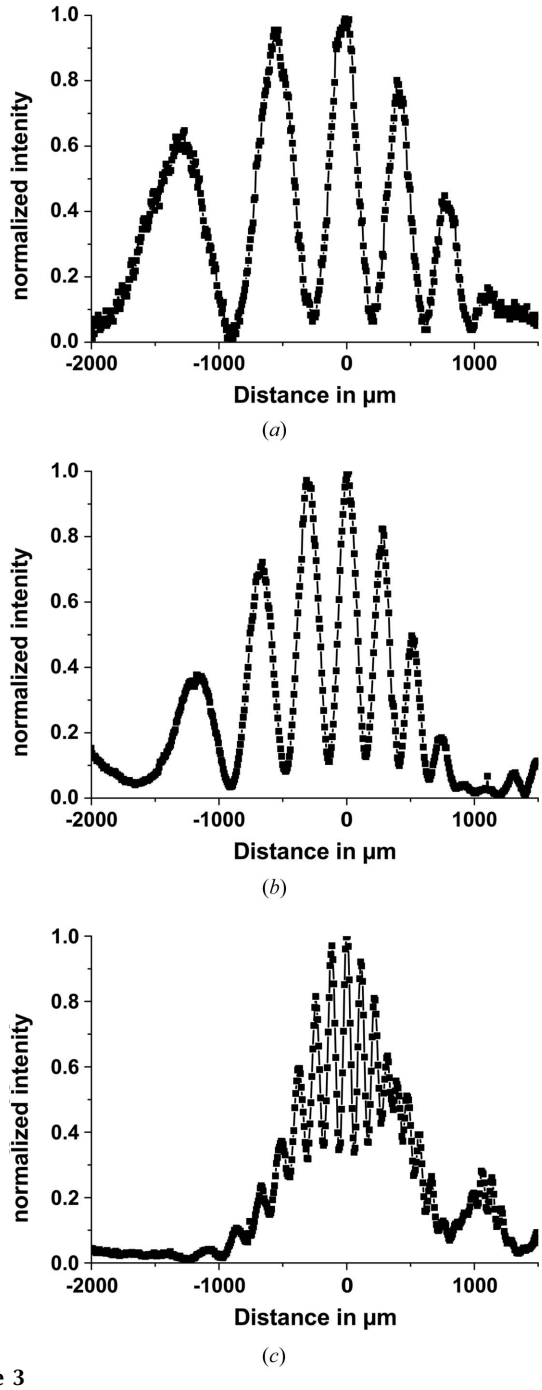

Figure 3
Normalized line profiles (vertical) extracted from the diffraction patterns in Figs. 2(*a*)–2(*c*) (solid lines joining the data points).

$$l_c = \lambda s/2\pi\sigma.$$

Here, s is the source-to-sample distance, σ is the source size of the synchrotron beam, γ is a prefactor, where $0 < \gamma < 1$ for fitting the measured data, and l_c is the spatial coherence length.

2.1. Monochromatic radiation

The experimental set-up is shown in Fig. 1. A double-crystal monochromator (DCM) selects a single energy out of the white spectrum emitted at the bending-magnet beamline BM05 at the European Synchrotron Radiation Source (ESRF), Grenoble (France). The bimirror under test was aligned at the goniometer. The X-ray interference pattern was converted into visible light by a fluorescence screen and was magnified by an optical microscope to a CCD camera (FRELON). The typical exposure time for an image was 1 min. The usable energy interval, 8 keV < E < 50 keV, was limited owing to the emission spectrum of the bending magnet (high limit) and the air absorption (low limit). Absorption was minimized by inserting pipes filled with helium in between the elements. Nevertheless, at both ends of the spectral range the data were already quite noisy. The lower limit of the incidence angle is given by the minimum separation of the direct beam and the reflected beam, because the large divergence of the diffracted beam in the case of small slits causes an overlap of the interference fringes with the direct beam. The upper limit of the incidence angle, 0.1°, was due to the limited translation of a pair of in-vacuum slits in between the FBM and the detector (see Table 1 for more details).

Table 1
Parameters of the FBM used in the experiment.

	Monochromatic beam	White beam
Mirror material	Silicon	Glass
Energy range	8–50 keV (discrete)	5–25 keV ('continuum')
Incidence angle	0.01° < α < 0.1°	0.02° < α < 0.18°
Mirror width	0.75 mm	0.5 mm
Mirror separation	5.0 mm	4.0 mm
Slit separation	3 μm < D < 20 μm	1.4 μm < D < 12 μm
Source distance	36 m	30 m
Distance z	5.50 m	1.3 m
Detector size	7.5 μm (pixel size)	5 μm (pinhole diameter)

2.2. White radiation

The experiment with white synchrotron radiation was performed at the bending magnet of the EDR beamline at BESSY synchrotron in Berlin (Germany) (Neissendorfer *et al.*, 1999; Leitenberger *et al.*, 2004; Pietsch *et al.*, 2001). An energy-dispersive detector (Xflash; Fa. Roentec) was used with an energy resolution of better than 200 eV at z = 1.3 m behind the FBM. The spatial resolution in the experiments, 5 μm, was governed by the diameter of a pinhole made in platinum and placed 1 cm in front of the detector. Young's fringe pattern could be recorded in an energy interval of 5–25 keV for different incident angles of the FBM. Here the energy resolution corresponds approximately to the spectral width of a pink undulator beam or a beam after monochromatization by a multilayer monochromator, whereas both cases are relevant for a number of applications. Table 1 gives more details.

3. Experimental results and discussion

We recorded the interference pattern of the FBM at different incidence angles (different D values) and at several energies. The evaluation of the fringe contrast from the measured

images shown in Figs. 2(*a*)–2(*c*) was carried out by extracting a vertical line of pixels which shows maximum intensity contrast. This is justified because the visibility can only be reduced by artefacts and cannot be increased. So the biggest visibility signifies a position at the FBM where the best experimental conditions are available. The numerical evaluation was carried out either by fitting equation (2) to the data or, in cases of insufficiently overlapping diffraction peaks, by determining the visibility near the central fringes of the diffraction pattern using the definition of V [equation (3)].

3.1. Problem of detector resolution

In our experiment the spatial resolution of the detector plays an important role. We need to measure the correlation between partial waves at large distances from each other, which corresponds to a large slit separation. Here the fringe distance becomes smaller and the quantitative determination of the fringe visibility is limited by the spatial resolution of the detector.

To estimate the maximum slit separation at a given detector resolution we assume a fringe spacing of $s > N_{\min} p$. Here, p is the pixel size (7.5 μm) and $N_{\min}$ is the minimum number of pixels still sufficient to not significantly reduce the measured visibility. The maximum slit separation can be found from $s = \lambda z/D > N_{\min} p$. Finally, $D_{\max} < \lambda z/N_{\min} p$. For $N_{\min} = 10$ and the experimental parameters given above, we obtain $D < 7.3\lambda$ (with D in μm and λ in Å). This relation is not always satisfied. It should be pointed out that the problem of detector resolution was not considered sufficiently in several papers about the quantitative determination of the coherence length of hard X-rays (Pfeiffer *et al.*, 2005; Leitenberger *et al.*, 2001, 2004).

When having only a few pixels within a fringe period, there is a significant decrease in the measured visibility owing to averaging over a large interval of the fringe period. As a result, the decay of the $V(D)$ curve for higher D is faster than it would be for higher detector resolution, and this results in a smaller l_c value.

The maximum measured visibility value in our experiments was $V_{\max} \simeq 0.8$. This maximum visibility seems to be the limitation of our actual experimental set-up. This value was obtained at the largest possible fringe distance corresponding to a small slit separation and long wavelength, where a visibility close to unity is expected.

3.2. Monochromatic radiation

Figs. 2(*a*)–2(*c*) show interference patterns of the reflected beams recorded at energies of 8, 15 and 40 keV at an incidence angle of 0.02°. The horizontal interference fringes with non-uniform spacing are superimposed by some artefacts caused by beamline components. The vertical stripes coincide with vertical lines seen in the image of the direct beam in Fig. 2(*d*). These artefacts are caused by scratches in Be vacuum windows at about 1.5 m downstream of the FBM. Owing to the illumination with narrow sources and the highly divergent beam, the local artefacts are strongly enlarged and pronounced compared with the image seen in the direct beam. The influence of scratches is less pronounced for higher energies owing to less interaction with the window material.

In experiments with higher-energy X-rays at incident angles above the critical angle, we found another effect. Here we observed simultaneously two different interference patterns (Fig. 1*b*). The upper pattern is created by the reflected beams as described earlier. A second interference pattern, located between the incident and the reflected beam, is created by the refracted part of the two beams. As sketched in Fig. 1(*b*), two refracted beams penetrating two mirrors leave the mirrors at the vertically cut surface.

From Snell's law, $n = 1 - \delta = \sin\beta_0/\sin\beta_{\rm refr}$, we find, with $\beta_{0,r} = 90° - \alpha_{0,r}$ at $E = 30$ keV, $\alpha_0 = 0.0625°$ and $\alpha_{\rm refr} = 0.0195°$, a value of $\delta_{\rm exp} = 5.22 \times 10^{-7}$. Here β_0 and $\beta_{\rm refr}$ are angles between the surface normal and the reflected and refracted beam, respectively. This is within our experimental errors with the tabulated value of $\delta_{\rm calc} = 5.37 \times 10^{-7}$. The small absorption in silicon at 30 keV allows this effect to be observed. The surface of the 'vertical' side walls of the small mirrors were extremely rough compared with the polished surface of the mirrors. This rough surface could not destroy the beam interference.

An interesting property of the interference pattern in the refracted beam is the following. For the refracted beam the effective dimensions of the slit are always smaller than those of the reflected beam, $D_{\rm refr} = \alpha_{\rm refr}(B - b) < \alpha_0(B - b)$. This effect is most pronounced just above the critical angle where $\alpha_{\rm refr}$ is almost zero. The intensity contrast of the interference fringes in a given set-up is determined by the separation of the two slits as seen by the incoming beam. The apparent beam compression as observed in the refracted beam gives higher fringe spacing than in the reflected beam. This may help to overcome limitations given by the lateral resolution of the detector and will be discussed below.

In the case of the reflected beam there is no pathlength difference between the two interfering beams (except minor differences owing to additional inclination between the two mirrors). However, in the refracted beam we have an optical pathlength difference Δl. This is because the beam refracted at the lower mirror (Fig. 1*b*) does not always pass inside the substrate but passes through the air gap of length $B - 2b$ in between the two mirrors. The optical pathlength difference is then given by $\Delta l = \delta_{\rm calc}(B - 2b)/\lambda$. Owing to the negative refraction index the optical pathlength of the lower beam is shorter by Δl. Taking the numerical values from the example using 30 keV radiation we find that $\Delta l \simeq 46$ wavelength units. Since we clearly observe interference fringes, the longitudinal coherence length, $l_l = \lambda^2/2\Delta\lambda$, of our beam must be larger than this value. We can easily estimate that the spectral resolution $\Delta\lambda/\lambda$ of the monochromator at 30 keV is much better than 8×10^{-3}, which is of course not very spectacular. We can further conclude that we would not see interference fringes in the white-beam experiment since the energy resolution in this experiment would be too low.

Fig. 4(*a*) shows the measured fringe visibility as a function of the slit separation D determined from the measurements at different energies between 8 keV and 40 keV. By fitting the

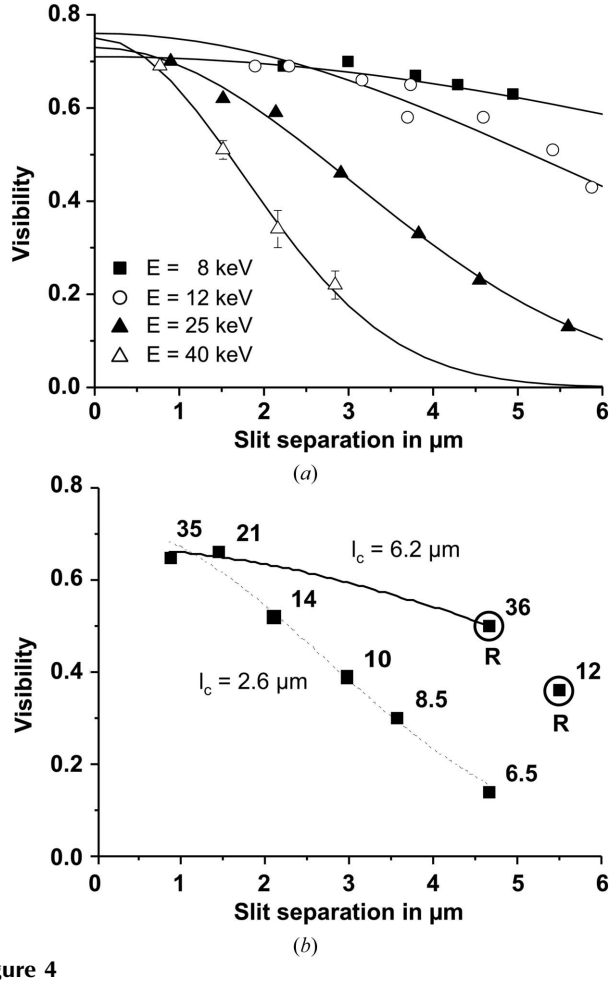

Figure 4
(*a*) Measured visibility as a function of slit separation at four beam energies. The solid lines show the best fit of equation (5) to the data. The data of the reflection interferograms were used. (*b*) Measured visibility and fit to equation (5) plotted as a function of the slit separation at 30 keV. Dotted line: reflected beam only; solid line: considering $s > 20p$ only. The number at each data point gives the fringe distance in number of pixels N and the points marked 'R' are obtained from the refracted beams.

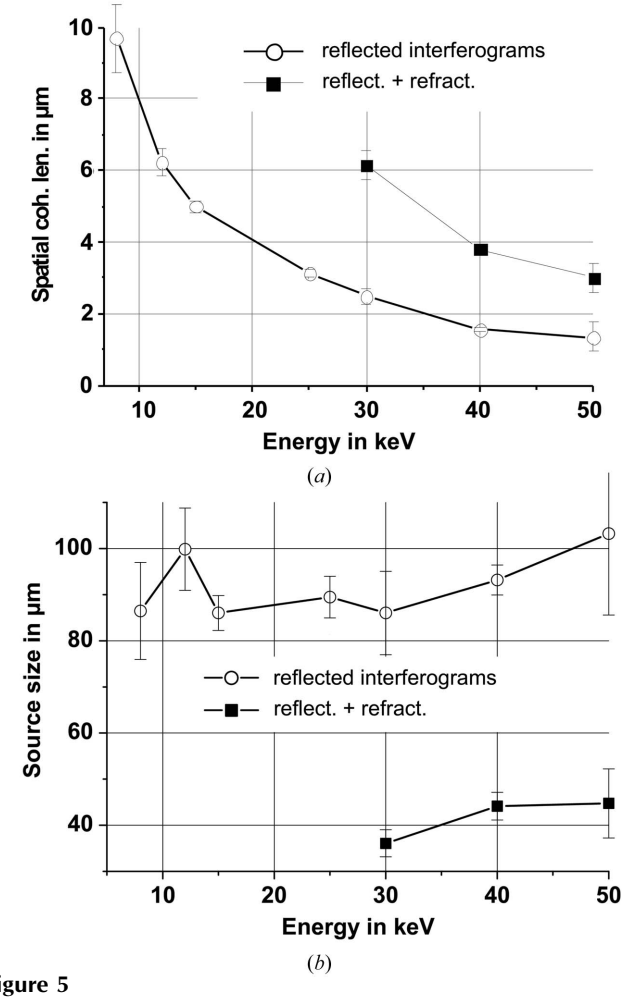

Figure 5
(*a*) Coherence length $l_c(E)$ determined from the $V(D)$ curves in Fig. 4. Open circles: all reflected interferograms; solid squares: reflected and refracted interferograms with $s > 20p$. (*b*) Size of the source point of synchrotron radiation obtained from l_c values according to equation (5).

measured visibility values to equation (5) we obtain the spatial coherence length l_c for each beam energy (see Fig. 5*a*).

At high energies we have available two visibility values measured at the same slit separation but with different fringe distances. For some D values we can compare the visibility measured in the reflected beam with that of the refracted beam. We briefly discuss the case of 30 keV radiation. In the reflected beam at $\alpha_i = 0.06^\circ$ we observed a fringe spacing s_{refl} = 49 µm (equivalent to $N = 6.5$ pixel) and in the refracted beam we have s_{refr} = 270 µm ($N = 36$ pixel). In terms of coherence measurements we need to consider the same 'slit' separation D = 4.6 µm for both experiments. While the visibility in the reflected beam is already strongly reduced by the small fringe distance, the refracted beam was not affected, and we have $V_{refl} = 0.14$ compared with $V_{refr} = 0.50$. Fig. 4(*b*) shows all visibility values measured at 30 keV. By fitting equation (5) to the visibility values obtained from the reflected beam we find that l_{coh} = 2.6 µm. Now we consider solely the visibilities obtained from interferograms of the reflected and the refracted beams with $s > 20p$. Thus resolution effects are minimized and we obtain l_{coh} = 6.2 µm, which is a factor of 2.3 larger than the first value. A similar result is obtained for 40 keV and 50 keV radiation (see solid squares in Fig. 5*a*).

Fig. 5(*b*) shows our results for the vertical source size σ. The source size at ESRF beamline BM5 has already been experimentally determined by two different methods (Kohn *et al.*, 2000; Guigay *et al.*, 2004). The value should be about 80 µm, which also agrees with the value of 87 µm calculated by the ESRF machine group. The σ values we obtained from the reflected beam measurements agree within our experimental errors with the values from the literature. Looking at the σ values obtained using the refracted beam, however, we could conclude that the X-ray source is only about 40 µm. The reason for this discrepancy is not yet clear.

3.3. White radiation

The results of three vertical line scans of the detector pinhole are shown in two-dimensional grey-scale plots in Fig. 6.

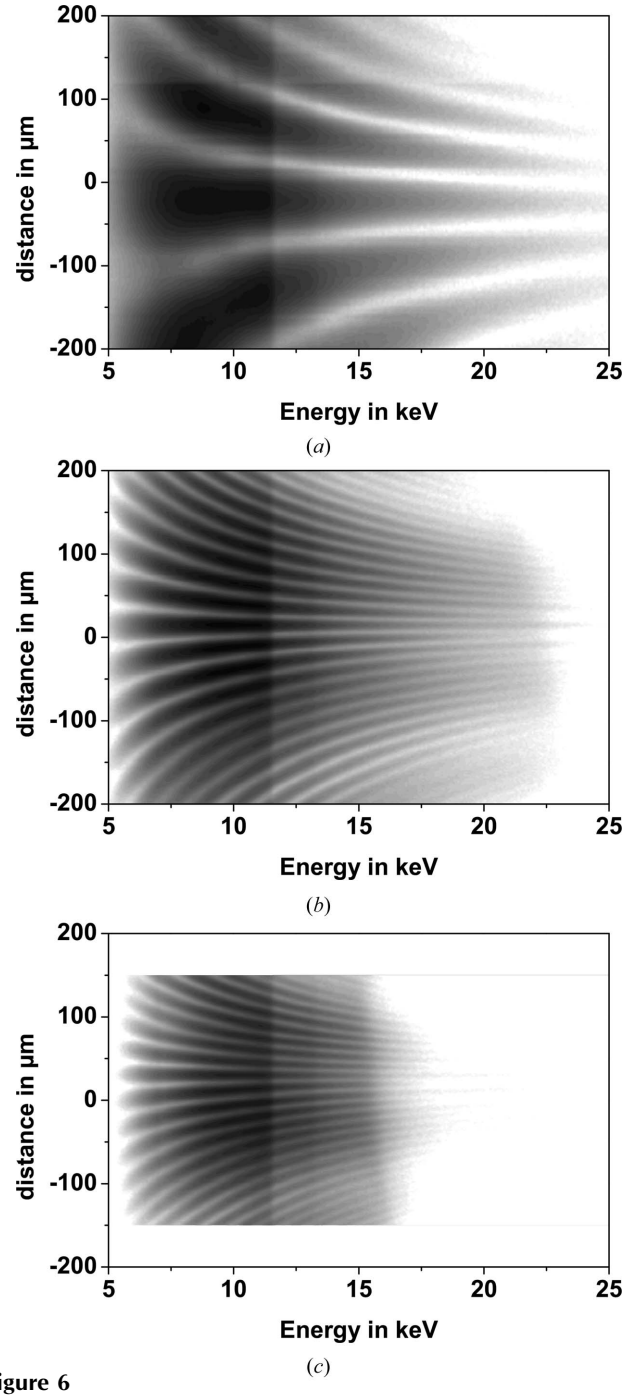

Figure 6
Diffraction pattern of a Fresnel bimirror at three different incident angles equivalent to (*a*) D = 1.4 µm, (*b*) D = 2.9 µm and (*c*) D = 7.3 µm slit separation (energy interval 5–25 keV). At ±200 µm from the centre, 200 energy spectra are shown in a logarithmic grey-scale map. Each horizontal line represents an energy spectrum measured through a 5 µm pinhole (black is high intensity).

A continuum of Young's fringes (vertically) can be seen as a function of energy. The fringe spacing decreases when changing from lower to higher X-ray energies.

In the interference pattern we see again the asymmetry (larger fringe spacing at lower reflection angles). The diffraction pattern is free of strong artefacts owing to partial transmission as observed in previous diffraction experiments

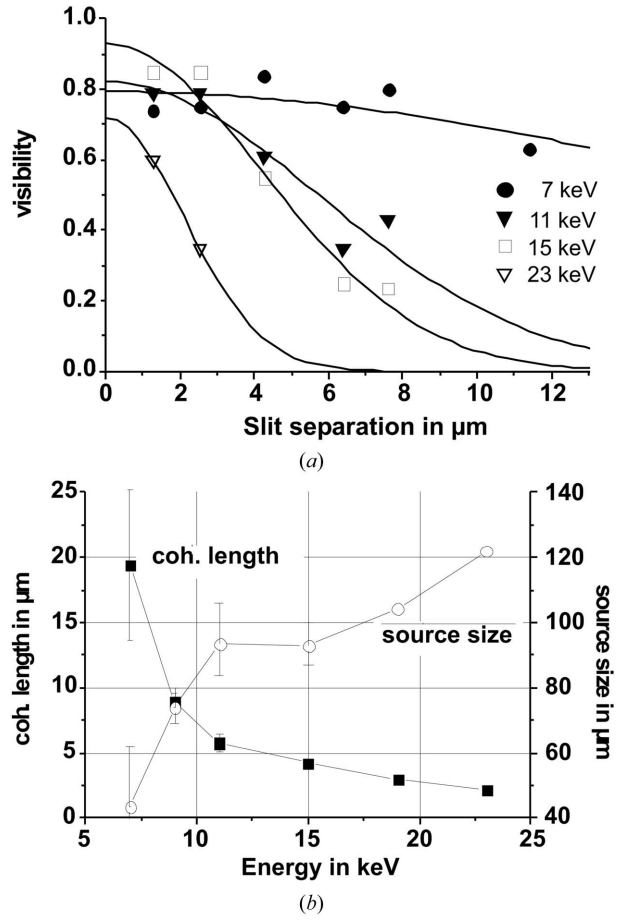

Figure 7
(*a*) Measured visibility as a function of slit distance at four beam energies. The solid lines show the best fit of equation (2) to the data. (*b*) Filled boxes: coherence length $l_c(E)$ determined from the $V(D)$ curve in (*a*). Open circles: size of the source point of synchrotron radiation obtained from l_c values according equation (5).

with small pinholes in thin metal foils (Leitenberger *et al.*, 2004). Nevertheless, some weak artefacts are seen at energies of the absorption edges of platinum (the material of the detector pinhole). They are visible in Fig. 6 as vertical lines of contrast at 11.5 keV and 13.3 keV. In the diffraction pattern in Fig. 6(*c*), recorded at $\alpha_0 = 0.18^\circ$, we can see a second intensity drop at about 16 keV. This edge is slightly changing its energy value with the height position of the detector. At this incidence angle the critical angle of total external reflection is already within the recorded energy range. At energies above the 'critical energy' for that particular α_0, the reflectivity decreases strongly.

The evaluation of the coherence properties of the white beam was carried out in a similar way as for the monochromatic beam. Again the fringe visibility was determined for a number of different slit distances D and beam energies (Fig. 7*a*). For that monochromatic diffraction, profiles were extracted from the measured data. Fig. 7(*b*) shows a summary of the experimentally determined spatial coherence length and vertical source size as a function of energy.

Since we have a detector resolution of 5 µm and a distance z = 1.3 m, our angular resolution of the detector is lower than

that in the monochromatic experiment by a factor of 2.8. Proof of our experimental results should be a constant source size for all measured energies since the X-ray emitting electron beam is always the same for all energies. As we see in Fig. 7(*b*), the source size of σ (7 keV) = 43 µm is much smaller than σ (23 keV) = 123 µm, where we used an interference pattern with much smaller fringe spacing. Of course the much larger fringe spacing at 7 keV gives a more realistic visibility value. The X-ray source size at a bending magnet of BESSY was measured to be 50 µm, as reported by Holldack *et al.* (2001).

3.4. Remarks on the quality of the FBM

After the preparation of the bimirror from an originally flat substrate we registered a small bending of the mirrors with respect to each other. The bending was initially determined by observing visible-light interferences of the small air gap between a flat reference plate and the bimirror sample. One could assume intuitively that a weak tilt of the two interfering wavefronts washes out any interference effect at ångstrom wavelengths. However, the fringe spacing of a FBM is defined only by the angular separation of the two source points seen from a point at the detector, and this quantity is independent of the tilt angle $\delta\alpha$ of both mirrors. Nevertheless, a tilt angle of about 30 arcsec is already visible in the X-ray experiments. The tilt mainly influences measurements at low divergence of the two reflected beams. It is mostly significant at short wavelengths of the incident beam and at large effective slit sizes. In both cases the diffraction pattern of the reflected and diffracted waves do not completely overlap at the detector position and hence the amplitudes of the two interfering waves are not equal. This causes a lower fringe contrast, especially at large distances from the centre of the diffraction pattern (see Fig. 8).

In the case of partial overlap of the two waves the measured visibility V is not constant within the interference pattern, and according to equation (4) it is not equal to the complex coherence factor μ_{12}. Here the prefactor takes into account the changing intensity distribution of the two partial waves. A look at the expression shows that, even at an intensity ratio of $I_1/I_2 = 0.6$, the correction factor is about 3% which is still acceptable for our needs, and we have neglected this correction in this paper. In the case of clearly separated interference maxima we determined the visibilities in the centre of the interference pattern using equation (3). The visibility determined at this position is approximately the same as that of an ideal FBM.

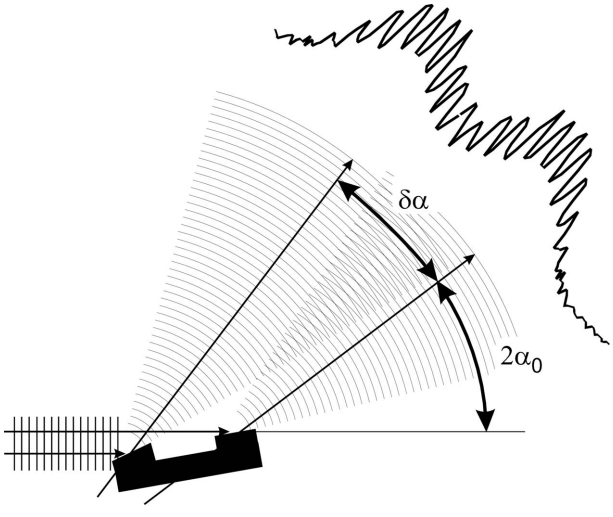

Figure 8
Outline of the FBM with two tilted mirrors, two inclined diffraction cones and a schematic interference pattern with two partially overlapping maxima.

4. Summary and conclusions

With a monolithic Fresnel bimirror we can characterize the coherence properties of X-rays by evaluating high-contrast interference patterns of energies up to 50 keV. We are able to determine the spatial coherence length and the source size of the X-ray beam in a large spectral range. Nevertheless, to obtain more accurate results the experimental set-up has to be improved in the following ways:

(i) The spatial resolution of the detector should be adequate for visibility measurements of interference patterns of about 20 points per fringe for the largest slit separation. For this purpose a smaller effective pixel size or a larger detector distances is necessary.

(ii) A FBM with a smaller or a zero tilt angle $\delta\alpha$ between the mirrors is needed to reduce the error caused by incomplete overlapping of the two diffraction patterns. Such a monolithic device from quartz is under preparation and will be tested in the near future.

(iii) Since the area of the approximated slits is of micrometre size, the properties of the beam are studied in a very local area. In order to exclude the influence of purely distributed inhomogeneties in optical elements producing artefacts in the beam profile and in the diffraction pattern, several experiments at different slit positions should be performed. For the characterization of the beam properties in larger areas, the grating technique presented by Pfeiffer *et al.* (2005) is more effective but requires very special gratings.

This work was supported by the German Ministry of Education and Research (05 KS4IPC/7). Additional financial support for beamline operation and instrumentation are kindly acknowledged: the Max Planck Institute for Colloids and Interfaces (Potsdam-Golm) and BESSY (Berlin). We thank E. Ziegler and his colleagues for preparing ESRF beamline BM05 for our needs. T. Sant (Universität Siegen) and R. V. Reddy (CAT Indore) are kindly acknowledged for their help at the experiments, and I. Vartanyants (HASYLAB Hamburg) for careful reading of the manuscript.

References

Aoki, S., Watanabe, N., Ohigashi, T., Yokosuka, H., Suzuki, Y., Takeuchi, A. & Takano, H. (2005). *Jpn. J. Appl. Phys.* **44**, 417–421.
Born, M. & Wolf, E. (1999). *Principles of Optics*, 7th ed. Cambridge University Press.
Fezzaa, K., Comin, F., Marchesini, S., Coïsson, R. & Belakhovsky, M. (1997). *X-ray Sci. Technol.* **7**, 12–23.

Goodman, J. W. (1985). *Statistical Optics.* New York: Wiley.
Guigay, J.-P., Zabler, S., Cloetens, P., David, C., Moksoa, R. & Schlenker, M. (2004). *J. Synchrotron Rad.* **11**, 476–482.
Holldack, K., Feikes, J. & Peatman, W. B. (2001). *Nucl. Instrum. Methods A*, **467–468**, 235–238.
Kohn, V., Snigireva, I. & Snigirev, A. (2000). *Phys. Rev. Lett.* **85**, 2745–2748.
Lang, A. R. & Makepeace, A. P. W. (1999). *J. Synchrotron Rad.* **6**, 59–61.
Leitenberger, W., Kuznetsov, S. M. & Snigirev, A. (2001). *Opt. Commun.* **191**, 91–96.
Leitenberger, W., Wendrock, H., Bischoff, L. & Weitkamp, T. (2004). *J. Synchrotron Rad.* **11**, 190–197.
Marchesini, S., Fezzaa, K., Belakhovsky, M. & Coïsson, R. (2000). *Appl. Opt.* **39**, 1633–1636.
Neissendorfer, F., Pietsch, U., Brezesinski, G. & Möhwald, H. (1999). *Meas. Sci. Technol.* **10**, 354–361.
Paterson, D., Allman, B. E., McMahon, P. J., Lin, J., Moldovan, N., Nugent, K. A., McNulty, I., Chantler, C. T., Retsch, C. C., Irving, T. H. K. & Mancini, D. C. (2001). *Opt. Commun.* **195**, 79–84.
Pfeiffer, F., Bunk, O., Schulze-Briese, C., Diaz, A., Weitkamp, T., David, C., van der Veen, J. F., Vartanyants, I. A. & Robinson, I. K. (2005). *Phys. Rev. Lett.* **94**, 164801.
Pietsch, U., Grenzer, J., Geue, T., Neissendorfer, F., Brezesinski, G., Symietz, C., Möhwald, H. & Gudat, W. (2001). *Nucl. Instrum. Methods A*, **467–468**, 1077–1080.
Pietsch, U., Panzner, T., Leitenberger, W. & Vartanyants, I. A. (2005). *Physica B*, **357**, 45–52.
Veen, J. F. van der & Pfeiffer, F. (2004). *J. Phys. Condens. Matter*, **16**, 5003–5030.